




SYNTHESIS OF ZEOLITE NaY FROM DEALUMINATED METAKAOLIN AS Ni SUPPORT FOR CO₂ HYDROGENATION TO METHANE

NOVIA AMALIA SHOLEHA¹, LAILATUL JANNAH¹, HANNIS NUR ROHMA¹, NURUL WIDIASTUTI¹,
DIDIK PRASETYOKO^{2,3*}, AISHAH ABDUL JALIL^{2,3}, AND HASLIZA BAHRUJI^{4*} 

¹Department of Chemistry, Faculty of Science, Institut Teknologi Sepuluh Nopember, Keputih, Sukolilo, Surabaya 60111, Indonesia

²Department of Chemical Engineering, Faculty of Chemical and Energy Engineering, Universiti Teknologi Malaysia, 81310 UTM, Skudai, Johor Bahru, Johor, Malaysia

³Centre of Hydrogen Energy, Institute of Future Energy, Universiti Teknologi Malaysia, Skudai, 81310 UTM, Skudai, Johor Bahru, Johor, Malaysia

⁴Centre of Advanced Material and Energy Science, University Brunei Darussalam, Jalan Tungku Link BE 1410, Brunei Darussalam

Abstract—The conversion of CO₂ into carbon feedstock via CO₂ hydrogenation to methane requires a stable catalyst for reaction at high temperatures. Zeolite NaY (abbreviated hereafter as NaY) synthesized from naturally occurring kaolin provides a stable support for Ni nanoparticles. Kaolin can be further dealuminated using sulfuric acid to reduce the Si/Al ratio, but the presence of the remaining sulfur is detrimental to the formation of NaY. The objective of the present study was to synthesize NaY from dealuminated metakaolin, using a method that minimizes the detrimental effects of sulfur, and to investigate the effect of its activity on CO₂ methanation. Kaolin from Bangka Belitung, Indonesia, was calcined at 720°C for 4 h to form metakaolin (M) and subsequently treated with sulfuric acid to form dealuminated metakaolin (DM). Excess sulfur was removed by washing with deionized water at 80°C. Zeolite NaY was then synthesized from the M and DM via a hydrothermal method; the relationship between morphology, structural properties, and the catalytic activity of NaY was determined for CO₂ methanation at 200–500°C. The presence of excess sulfur following dealumination of metakaolin produced NaY with small surface area and porosity. After Ni impregnation, the synthesized NaY exhibited significant catalytic activity and stability for the reaction at 250–500°C. Analysis by scanning electron microscopy and high-resolution transmission electron microscopy showed the formation of well-defined octahedral structures and large surface areas of ~500 m²/g when NaY was synthesized using DM. Catalytic activity indicated significant conversion of CO₂ (67%) and CH₄ selectivity (94%) of Ni/NaY from DM in contrast to only 47% of CO₂ conversion with 77% of CH₄ selectivity for Ni/NaY synthesized from M. Dealuminated metakaolin also produced robust NaY, which indicated no deactivation at 500°C. The combination of well-defined crystallite structures, large surface area, and small Al contents in NaY synthesized from DM helped in CO₂ conversion and CH₄ selectivity for the reaction at 200–500°C.

Keywords—CO₂ methanation · Dealuminated metakaolin · Kaolin · Metakaolin · Ni nanoparticles · Zeolite NaY

INTRODUCTION

CO₂ methanation to CH₄ using renewable H₂ is a pathway to transform CO₂ into value-added carbon feedstock (Aziz et al. 2015). The reaction requires high temperatures (200–450°C) and the presence of active Ni nanoparticles (Fukuhara et al. 2017). Hydrogenation of CO₂ to methane is thermodynamically feasible at ambient pressure (Ewald et al. 2019) in contrast with CO₂ hydrogenation to methanol, which requires a high-pressure system (Bahruji et al. 2016). The critical aspect in the design of a robust catalyst is that it must have high catalytic activity and stability over a wide temperature range in order to prevent catalyst deactivation. Zeolite Y, ZSM-5, USY, zeolite 5A, and BEA have been investigated as supports for CO₂ hydrogenation to methane with Ni metal nanoparticles added to increase the conversion and selectivity toward methane (Graça et al. 2014; Westermann et al. 2015; Quindimil et al. 2018). As a weakly acidic gas, the adsorption of CO₂ is improved by increasing the basicity and the surface area of the zeolite (Walton et al. 2006). Replacing the compensating cation in zeolite with an alkali metal cation alters the charge and

the density of framework oxygen in the zeolite lattice and contributes to an increase in zeolite basicity (Quindimil et al. 2018; Bacariza et al. 2019). Reducing the amount of Al in the framework consequently decreases the zeolite basicity and weakens the C–O bond for high CO₂ conversion (Bacariza et al. 2019).

Faujasite (FAU)-type zeolite with a Si/Al ratio of 1.5 is also known as zeolite NaY and has been investigated widely as an adsorbent in gas storage (Dong et al. 2007), as a catalyst for hydrocracking reactions (Mu et al. 2019), and as support for metal or metal oxide nanoparticles in various catalytic reactions such as CO₂ hydrogenation, biodiesel production, and glucose isomerization to fructose (Du et al. 2018; Graça et al. 2018; Bacariza et al. 2019). Hydrothermal synthesis of zeolite from clay minerals produces a zeolite with a uniform crystal structure. Dry-gel and steam-assisted methods, however, provide a facile and scalable pathway for the green synthesis of zeolite (Weitkamp and Hunger 2005; Ashgari et al. 2019; Chen et al. 2020). Naturally occurring materials such as clay minerals, stone, and fly ash have also been investigated as alternative sources of silica and alumina (Doyle et al. 2017). The conversion of natural pyrophyllite as a new clay source via facile alkaline treatment produces hydroxysodalite zeolite with enhanced surface area and porosity (Gaidoumi et al. 2018).

* E-mail address of corresponding author: didikp@chem.its.ac.id
DOI: 10.1007/s42860-020-00089-3

Kaolin is a clay material consisting largely of kaolinite ($\text{Al}_2\text{O}_3 \cdot 2\text{SiO}_2 \cdot 2\text{H}_2\text{O}$) and has been investigated as a precursor for zeolite synthesis (Li et al. 2017; Wang et al. 2018). Kaolin obtained from Bangka Belitung, Indonesia, was previously converted to Zeolite HX and sodalite, which showed potential as an acid catalyst and adsorbent for the removal of heavy-metal pollutants from water (Ifitahiyah et al. 2019; Wahyuni et al. 2019). The thermal treatment of kaolin between 550 and 950°C produced active amorphous metakaolin (Kovo et al. 2009; Sperinck et al. 2011; Qoniah et al. 2015). Metakaolin can be further dealuminated with an inorganic acid such as HCl, H_2SO_4 , or HNO_3 to reduce the concentration of aluminum in the resulting zeolite (Colina and Llorens 2007; Alaba et al. 2017; Sri Rahayu et al. 2018). A large concentration of sulfuric acid enhances the dissolution of aluminum in kaolin; but, the remaining sulfur in kaolin also affects the structural properties of the zeolite that is synthesized (Alaba et al. 2017; Sri Rahayu et al. 2018).

In the present study, the aim was to establish the promotional effect of dealuminated metakaolin for the production of NaY with a large surface area in order to enhance stability and catalytic activity for CO_2 methanation, and to correlate CO_2 conversion and CH_4 selectivity with the surface area, the crystallite structure, and the Si/Al ratio of NaY in order to demonstrate the advantages of dealumination and complete removal of sulfur from metakaolin for the synthesis of NaY.

EXPERIMENTAL

Materials

Materials used in the experiments were kaolin, consisting primarily of kaolinite ($\text{Al}_4(\text{Si}_4\text{O}_{10})(\text{OH})_8$), obtained from Bangka Belitung Island, Indonesia, 57% SiO_2 and 22% Al_2O_3 , Ludox® HS-40 colloidal silica (30% SiO_2 ; 70% H_2O , Sigma Aldrich, Darmstadt, Germany), sodium hydroxide ($\geq 99\%$ NaOH, Merck KGaA, Darmstadt, Germany), deionized water (UD Sumber Ilmiah Persada, Surabaya, Indonesia), sulfuric acid (98% H_2SO_4 , Smart-Lab, Tangerang, Indonesia), hydrofluoric acid (48% HF, Sigma Aldrich, Darmstadt, Germany), nitric acid (65% HNO_3 , Merck KGaA, Darmstadt, Germany), and $\text{NiNO}_3 \cdot 6\text{H}_2\text{O}$ (Sigma Aldrich, Darmstadt, Germany).

Preparation of Metakaolin and Dealuminated Metakaolin

Kaolin was transformed to metakaolin by calcination at 720°C for 4 h (Li et al. 2010) and labeled as M (metakaolin). Dealumination of metakaolin was carried out by adding 1 g of metakaolin powder to 1 mL of 6 M sulfuric acid solution. The mixture was stirred at 90°C for 2 h to form an homogeneous mixture. The mixture was dried at 110°C for 12 h and calcined at 550°C for 2 h in a muffle furnace, and labeled as SM (sulfuric acid-soaked metakaolin). The SM was washed with deionized water at 80°C to reduce the concentration of sulfur, and labeled as DM (dealuminated metakaolin). After 2 h, the solution was cooled and filtered and then the residue was dried in an oven at 105°C for 6 h. The M, SM, and DM were used as precursors for the synthesis of NaY.

Synthesis of Zeolite NaY

Zeolite NaY was synthesized using a hydrothermal method in an autoclave with a Teflon liner; the starting materials were: M, SM, and DM with molar composition of 6 Na_2O :10 SiO_2 :1 Al_2O_3 :180 H_2O (Ginter et al. 1992). 3.2 g of NaOH was stirred into 22.3 mL of deionized water in a propylene bottle for 15 min or until dissolved. Then 2.83 g of metakaolin was added to this NaOH solution and stirred gently for 30 min. 14.37 g of LUDOX was added and the mixture stirred for 30 min. The resulting mixture was left to age for 24 h at room temperature followed by hydrothermal processing at 100°C for 24 h. The gel was filtered and washed with deionized water until the pH reached 7 in order to remove the remaining NaOH. The powder was dried in air in an oven at 105°C for 5 h and labeled as NaY-M. The procedures were repeated to synthesize NaY from SM and DM and were labelled as NaY-SM and NaY-DM, respectively.

Preparation of Ni/NaY Catalyst

A 5 wt.% loading of Ni nanoparticles was deposited on the as-synthesized NaY via the wetness impregnation technique. 0.260 g of $\text{NiNO}_3 \cdot 6\text{H}_2\text{O}$ was added to 10 mL of water to form a Ni solution which was added dropwise to 1 g of NaY. The mixture was mixed and dried at 110°C for 16 h followed by calcination at 550°C for 3 h.

Characterization

Elemental compositions of M, SM, and DM were determined by X-ray fluorescence (XRF) analysis using a PANalytical MiniPal 4 Sulfur (PANalytical B.V., Almelo, The Netherlands) instrument operating at a maximum voltage of 30 kV and a maximum current of 1 mA. The samples were pressed into pellets and inserted into the instrument sample holder and held there for 10 min. Organic functional groups were identified in KBr pellets (1:9 sample:KBr) of the samples using FTIR spectroscopy (Shimadzu FTIR-8400S, Tokyo, Japan) in the range 4000–400 cm^{-1} . The crystalline phases of the materials were determined from X-ray powder diffraction (XRD) patterns ($\text{CuK}\alpha$, 40 kV, 30 mA) over the range from 5 to 50°2 θ at a scan speed of 0.04°2 θ /s using a Philips-Binary X'Pert X-ray diffractometer (PANalytical B.V., Almelo, The Netherlands). The morphology of the samples was determined using scanning electron microscopy (SEM). The sample was placed on a carbon tape base and coated with Au for 15 min at a pressure of 6×10^{-2} mBar and analyzed using a SEM (ZEISS EVO MA 10, Carl Zeiss Microscopy GmbH, Jena, Germany). Energy dispersive X-ray spectroscopy (EDX) using a BRUKER 129 EV spectrometer (Bruker Nano GmbH, Berlin, Germany) was used to determine the element compositions. Surface area and pore-size distribution of the catalyst were calculated from nitrogen adsorption-desorption isotherms obtained using a Beckman Coulter SA 310 instrument (Beckman Coulter Inc., Fullerton, California, USA). The sample was degassed for 3 h at 150°C prior to analysis. To provide detailed morphological and compositional information at micro- and nano-scales, high-resolution field emission transmission electron microscopy (HRTEM) at 200 kV was used (Tecnai G² F20 S-TWIN, FEI Company, Hillsboro, Oregon, USA). For TEM analysis, the material was ground and mixed with water; then 2 mL of

the resulting suspension was placed on the TEM grid and dried. The instrument was equipped with a high-resolution digital camera providing a maximum resolution of 0.2 Å which enabled detailed observation of the crystal lattice, diffraction patterns, and lattice *d* spacing with the help of the *Digital Micrograph* software. The actual concentration of Ni on Ni/NaY catalysts was determined using atomic absorption spectroscopy (AAS) (ThermoFisher Scientific iCE 3000 Series AAS, Thermo Electron Manufacturing Ltd, Cambridge, UK). 0.2 g of the catalyst was dissolved in 2 mL of HF under stirring and heating at 80°C to dissolve the catalysts. 10 mL of HNO₃ was then added to the solution and evaporated to reduce the volume of the solution. The solution was further diluted with deionized water to a fixed volume of 50 mL and analyzed.

Catalytic Testing

Catalytic activities of Ni/NaY catalysts were determined for CO₂ methanation using a laboratory-assembled packed-bed-continuous flow reactor at 200–500°C. 0.2 g of catalyst was placed in a stainless steel tube and annealed under air flow at 500°C for 1 h followed by a H₂ stream at 500°C for 3 h. CO₂ and H₂ were flowed in stoichiometric ratios of 1:4 at 25 mL/min. The gas composition was analyzed using an online 7820A Agilent gas chromatograph (GC) (Agilent Technologies Inc., Shanghai, China), equipped with a thermal conductivity detector (TCD). The conversion and the selectivity of the products were calculated using the following equations:



$$X_{\text{CO}_2} = 1 - \frac{M_{\text{CO}_2}}{M_{\text{CH}_4} + M_{\text{CO}} + M_{\text{CO}_2}} \quad (2)$$

$$S_{\text{CH}_4} = \frac{M_{\text{CH}_4}}{M_{\text{CH}_4} + M_{\text{CO}}} \quad (3)$$

$$Y_{\text{CH}_4} = X_{\text{CO}_2} \cdot S_{\text{CH}_4} \quad (4)$$

where X_{CO_2} (%) is the conversion of carbon dioxide, S_{CH_4} is the selectivity for methane, Y_{CH_4} is the yield of methane, and M is the number of moles of the respective gases.

RESULTS AND DISCUSSION

Elemental Analysis of Kaolin Using XRF

The elemental compositions of M, SM, and DM were determined using XRF (Table 1). Metakaolin consisted of 59.4% SiO₂ and 35.5% Al₂O₃ with trace amounts of P₂O₅, K₂O, CaO, TiO₂, V₂O₅, Cr₂O₃, MnO, Fe₂O₃, and BaO. Treatment with sulfuric acid caused the disappearance of P₂O₅ and Cr₂O and the reduction of all the metal-oxide impurities. The sulfur content was analyzed at 27.5% following dealumination treatment and the concentrations of Al₂O₃ and SiO₂ were reduced to 25.6% and 41.9%, respectively. Washing the SM sample with water reduced significantly the concentration of sulfur to 7.8% and increased the SiO₂ and Al₂O₃ concentrations to 29.5% and

Table 1. Elemental analysis (wt.%) by XRF of metakaolin (M), sulfuric acid-soaked metakaolin (SM), and dealuminated metakaolin (DM)

Oxide	M	SM	DM
Al ₂ O ₃	35.5	26.4	29.5
SiO ₂	59.4	41.9	58.2
P ₂ O ₅	0.88	0	0
K ₂ O	2	1.7	2.05
CaO	0.31	0.3	0.24
TiO ₂	0.35	0.26	0.32
V ₂ O ₅	0.02	0.03	0.03
Cr ₂ O ₃	0.063	0	0.033
MnO	0.041	0.031	1.95
Fe ₂ O ₃	2.07	1.79	0.1
BaO	0.25	0.09	0.1
SO ₃	0	27.5	7.48

58.2%, respectively. The SiO₂/Al₂O₃ ratio of DM sample increased to 1.97 compared to M at 1.67.

Infrared Analysis

Kaolin, M, SM, and DM were analyzed by FTIR to provide evidence for structural changes in the kaolinite following calcination and dealumination (Fig. 1). Results revealed an adsorption band at ~536 cm⁻¹, indicating the Al–O bond vibration in Al[O(OH)]₆. The absorption band that appeared at ~1115–1008 cm⁻¹ was associated with the vibration of Si–O–Si bonds (Qoniah et al. 2015). The vibration peaks of Al–OH appeared at ~795 and 697 cm⁻¹ and the vibration peaks of Si–O bonds were observed at 469 and 430 cm⁻¹ (Alkan et al. 2005). Following calcination at 500°C, the transformation of kaolin to metakaolin was observed by the disappearance of the features assigned to Al–O and Si–O–Si bonds in the kaolin framework. The metakaolin showed a broad absorption peak centered at 1095 cm⁻¹, which corresponded to the vibration of the Si–OT symmetric group (T is Si or Al). The absorption band at 810 cm⁻¹ corresponded to Si–OT bond vibration and the band that appeared at 472 cm⁻¹ was assigned to the Si–O vibrational bond (Ptáček et al. 2011). The broad hydroxyl–OH peak observed in M at 3600 cm⁻¹ showed significant reduction in intensity due to dehydroxylation and the removal of adsorbed water during annealing treatment. Dehydroxylation occurred based on the following reaction:



During calcination of kaolin at high temperatures, 1.5 moles of H₂O was removed for every mole of kaolin that was converted into metakaolin via the process described as dehydroxylation (Bessa et al. 2017).

Metakaolin treated with sulfuric acid showed an absorption band at 3396 cm⁻¹, corresponding to adsorbed water (Rasouli et al. 2015). The analysis also revealed the Si–O peak shifted toward a higher wavenumber at ~1170 cm⁻¹ due to the

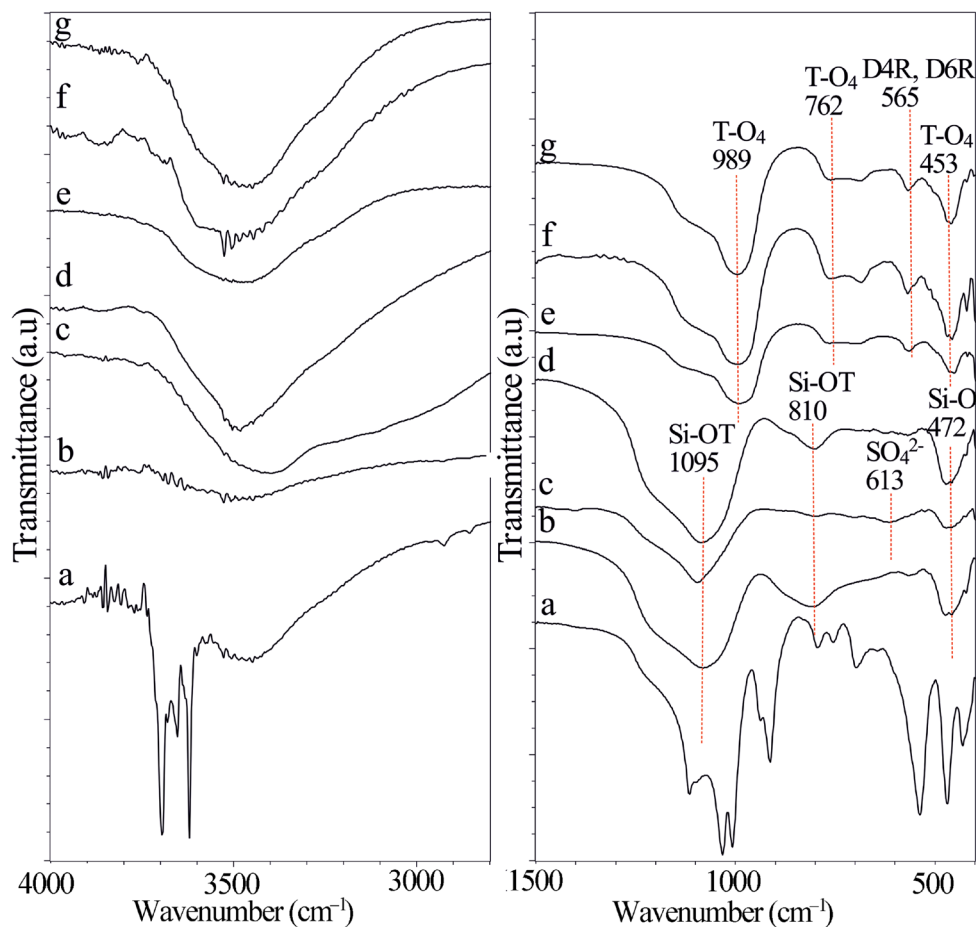


Fig. 1. IR analysis of: **a** kaolin, **b** metakaolin (M), **c** sulfuric acid-soaked metakaolin (SM), and **d** dealuminated metakaolin (DM), and zeolite NaY synthesized from **e** M, **f** SM, and **g** DM

asymmetric-symmetric stretching vibration of sulfate (SO_4^{2-}). The Si-OT vibration observed at 810 cm^{-1} in metakaolin also disappeared after sulfuric acid treatment, implying that the interaction between Si and sulfur followed the dealumination process. The disappearance of the Si-OT peak was also accompanied by the formation of an adsorption band at $\sim 613\text{ cm}^{-1}$, corresponding to the symmetric vibration of sulfate anions (Kloprogge et al. 2001). The dealuminated metakaolin showed the reappearance of the Si-OT peak at 810 cm^{-1} together with the reduced intensity of the sulfate peak at 613 cm^{-1} , suggesting the removal of sulfur following washing of SM.

Infrared analysis of the NaY synthesized from M, SM, and DM (Fig. 1) revealed that all the adsorption peaks associated with the kaolin at ~ 541 , 913 , and 1107 cm^{-1} disappeared. The peak observed at 453 cm^{-1} indicated the vibration band of TO_4 ($T = \text{Si, Al}$), and the peak which appeared at $500\text{--}600\text{ cm}^{-1}$ indicated the external vibration of the double four-membered ring (D4R) and double six-membered ring (D6R). The symmetrical internal and external vibrations of the O-T-O bonds were observed at $650\text{--}820\text{ cm}^{-1}$ and the asymmetric stretching vibrations of the T-O-T bonds were observed at $950\text{--}1250\text{ cm}^{-1}$. These

results were consistent with the previous studies which showed that the adsorption bands of zeolite Y appeared at 460 , 565 , 685 , 780 , and 1010 cm^{-1} (Holmberg et al. 2003).

XRD Analysis

The crystalline phase of kaolin was identified using XRD (Fig. 2a) with diffraction peaks appearing at 12.6 , 20.43 , 24.94 , 38.46 , and $45.54^\circ 2\theta$. Annealing of kaolin at 720°C showed the disappearance of the kaolin diffraction peaks due to the transformation of the kaolin crystalline structure into amorphous aluminosilicate. The annealing treatment also showed the formation of typical quartz peaks at ~ 19.6 and $26.64^\circ 2\theta$ (Kahraman et al. 2005) as the result of structural changes during the dehydroxylation process. No significant differences were found in the diffraction pattern of metakaolin following treatment with sulfuric acid.

The formation of NaY from M, SM, and DM was also analyzed using XRD (Fig. 2b). The diffraction patterns were in accordance with the JCPDS No. 39-1380 of NaY with the main peaks appearing at 6.31 , 10.31 , 12.31 , 15.92 , 19.01 , 20.71 , 24.06 , 27.52 , and $31.95^\circ 2\theta$ ($\text{CuK}\alpha$). Sodalite was produced commonly during the synthesis of NaY with the

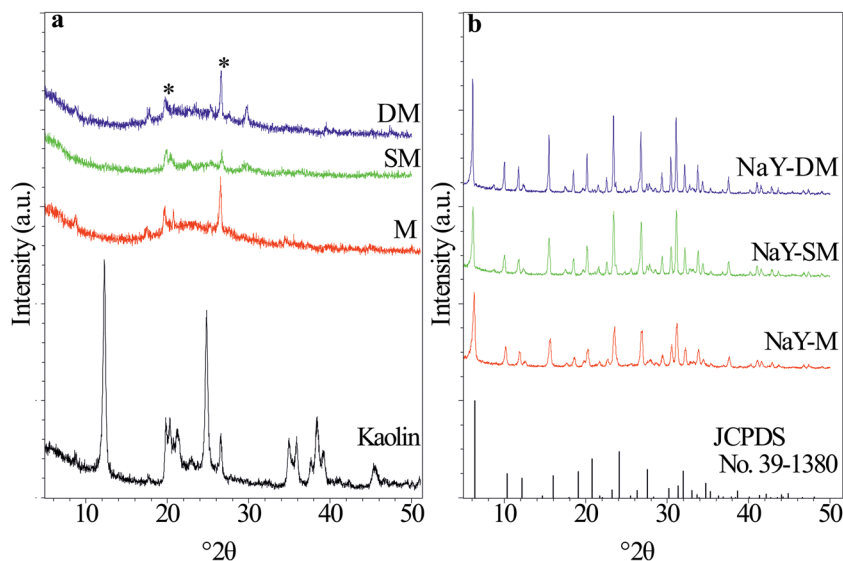


Fig. 2. XRD patterns of **a** kaolin, metakaolin (M), sulfuric acid-soaked metakaolin (SM), and dealuminated metakaolin (DM); **b** zeolite NaY synthesized from metakaolin, NaY-M; sulfuric acid-soaked metakaolin, NaY-SM; and dealuminated metakaolin, NaY-DM. *quartz SiO₂

characteristic peaks at ~ 14.20 , 24.43 , 31.79 , 34.85 , and $43.01^\circ 2\theta$ (Luo et al. 2016). However, no peaks associated with sodalite were observed in the XRD patterns of the zeolites synthesized here, indicating the formation of high-purity NaY from kaolin. The crystallite size of NaY (Table 2) was calculated using the Scherer equation based on the FWHM of the (111) peak at $6.31^\circ 2\theta$. The crystallite size of NaY-DM produced from dealuminated metakaolin was ~ 81 nm, which was significantly larger than NaY-SM at ~ 40 nm and NaY-M at ~ 21 nm.

N₂ Adsorption-desorption Analysis

The textural properties of NaY were determined using the N₂ adsorption-desorption method. The adsorption-desorption

isotherms of all NaY produced from M, SM, and DM (Fig. 3) were of type I, as indicated by the sharp increase in the isotherm at low P/P_0 before reaching steady state. The type I isotherm is a typical adsorption for NaY and it implies that the adsorption of nitrogen occurs within the micropores of the framework (Feng et al. 2019). The surface area and the pore volume of NaY synthesized from M (Table 3) were $376 \text{ m}^2/\text{g}$ and $0.015 \text{ cm}^3/\text{g}$, respectively. The surface area of NaY synthesized from SM was reduced significantly to $\sim 260 \text{ m}^2/\text{g}$, suggesting that the high concentration of sulfur in SM was detrimental to the formation of NaY. Reducing sulfur concentration in the sulfuric acid-soaked metakaolin with water at 80°C prior to the synthesis of NaY, however, significantly improved the surface area of NaY to 505

Table 2. Summary of the catalytic performances of Ni catalysts for CO₂ methanation reactions

Metal	Support	Reaction condition		Catalytic performance		Ref.
		<i>T</i> (°C)	<i>P</i> (atm)	<i>X</i> _{CO₂} (%)	<i>S</i> _{CH₄} (%)	
20% Co	KIT-6	300	1	46.7	99.5	Zhou et al. (2014)
	SiO ₂	300	1	28.1	98.3	
60% Ni	Al ₂ O ₃	300	1	17.5	64.3	Frusteri et al. (2017)
48% Ni	MgO	300	1	16.7	61.6	
70% Ni	HT	300	1	5	55.4	Atzori et al. (2017)
5% Ni	CeO ₂	300	1	48	97	
15% Ni	CeO ₂	300	1	66	98	
35% Ni	CeO ₂	300	1	57	98	
15% Ni	USY	450	1	72.8	96.4	Bacariza et al. (2018)
15% Ni	MCM-41	450	1	75.8	97	
15% Ni	SBA-15	450	1	71.4	95.6	
14% Ni	USY	350	1	63.9	65.3	Azzolina-Jury et al. (2017)
5% Ni	ZSM-11	350	1	69	68	

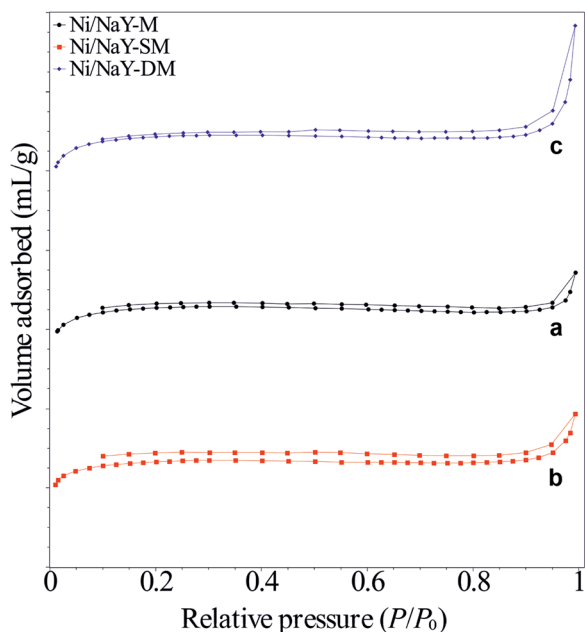


Fig. 3. N_2 adsorption-desorption isotherms of zeolite **a** NaY-M, **b** NaY-SM, and **c** NaY-DM

m^2/g and the pore volume to $0.304 \text{ cm}^3/g$ (sample NaY-DM, Table 2).

Morphology Analysis of Ni/NaY

Surface morphologies of zeolites NaY-M, NaY-SM, and NaY-DM were characterized using SEM analysis. The SEM image of NaY-M (Fig. 4a) synthesized from M revealed the formation of zeolite with non-uniform shape consisting of spherical and randomly shaped crystallites. Following dealumination with sulfuric acid, the NaY crystallites were transformed into octahedral structures with variation in the aggregate size. The dealuminated metakaolin as the NaY precursor revealed more uniform and well-defined octahedral structures. The aggregates of NaY-DM also appeared larger than NaY-SM and NaY-M as shown by the crystallite sizes (Table 3) calculated from the XRD analysis.

Images from TEM-EDX analysis of NaY-M and NaY-DM following impregnation with 5 wt.% Ni (Fig. 5a,c) revealed the homogeneous dispersion of Ni nanoparticles on NaY. HRTEM analysis of 5 wt.% Ni/NaY (Fig. 5b) also revealed well dispersed Ni nanoparticles with an average diameter of

2.6 nm and an interplanar distance of 0.242 nm, which corresponded to the NiO(111) crystal plane (Rakshit et al. 2013). No significant differences between the sizes of Ni nanoparticles were observed when NaY-M and NaY-DM were used as supports.

Catalytic Activity

Detailed characterization of synthetic NaY-DM showed increased surface area and pore volume and the formation of well-defined crystal structures. The catalytic activity of NaY was also investigated following impregnation with Ni nanoparticles for CO_2 methanation. Ni nanoparticles were also impregnated into NaY-M to provide evidence for the promotional effect of dealuminated metakaolin as a precursor to NaY catalytic activity. All the catalysts were pre-reduced at $500^\circ C$ for 3 h prior to the reaction in order to reduce NiO to Ni. The catalytic activity of Ni/NaY-M and Ni/NaY-DM at $400^\circ C$ (Table 3), with CH_4 and CO being the only products analyzed from the reaction, revealed a 67% conversion of CO_2 on Ni/NaY-DM compared to just 47% for Ni/NaY-M. Ni/NaY-DM also showed high selectivity for conversion to CH_4 at 94% while only 77% of methane selectivity was observed for Ni/NaY-M. Note that the control reactions were also carried out using a blank reactor and a bare Ni catalyst without any support and which showed negligible activity towards CO_2 methanation. The results exhibited the important role of the NaY support to enhance the activity of Ni by increasing the dispersion of Ni nanoparticles. The presence of Ni was crucial in providing the active sites for CO_2 dissociation, with the particle size and the amount of Ni loading affecting CO_2 conversion and product selectivity (Zhang et al. 2019). Impregnation of supporting material with a large loading of Ni produced large nanoparticles due to the sintering process that occurred during high-temperature calcination (Atzori et al. 2017). A review of previous investigations into Ni catalysts for CO_2 methanation (Table 4) indicated that high Ni loading (>50 wt.%) showed only ~5–17% of CO_2 conversion (Frusteri et al. 2017); reducing the Ni loading to only 5 wt.%, meanwhile, and increased significantly the CO_2 conversion to ~70% (Atzori et al. 2017; Azzolina-Jury et al. 2017). The actual amounts of Ni on the catalysts were determined using AAS (Table 4) and the results were ~6.3 wt.% in Ni/NaY-DM and ~4.6 wt.% in Ni/NaY-M. The values were slightly different when the initial loading of impregnated Ni was 5% wt. (due to experimental error during the AAS analysis), though the result showed the efficiency of the impregnation method for the deposition of Ni on NaY support.

Table 3. Textural properties of NaY synthesized from M, SM, and DM

Sample	Ratio Si/Al ^a	Crystallite size ^b (nm)	S_{BET} (m^2/g)	Pore volume (cm^3/g)	Pore radius (\AA)
NaY-M	1.21	28	376	0.015	19.74
NaY-SM	1.28	40	260	0.021	19.13
NaY-DM	1.32	81	505	0.045	19.14

^a Determined using EDX analysis; ^b determined using XRD

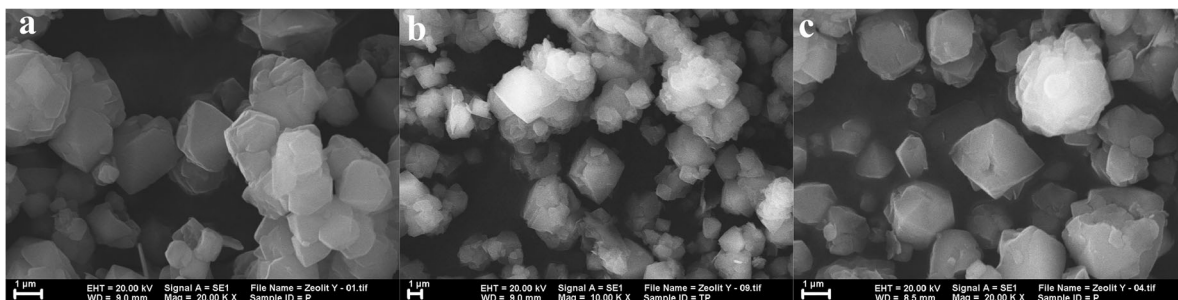


Fig. 4. SEM images of zeolite NaY from **a** metakaolin, NaY-M, **b** sulfuric acid-soaked metakaolin, NaY-SM, and **c** dealuminated metakaolin, NaY-DM. Scale bars: 1 μm

Catalytic activity of Ni/NaY-M and Ni/NaY-DM catalysts were also investigated at different reaction temperatures in the range 200–500°C (Fig. 6). The catalysts showed negligible activity for the methanation reaction at 200°C. Increasing the temperature to 250°C enhanced the CO₂ conversion of Ni/NaY-DM catalyst to 13%, though Ni/NaY-M showed only ~3% of CO₂ conversion. CO₂ conversion was improved significantly when the temperatures were increased to 400°C; Ni/NaY-DM exhibited much greater conversion and CH₄ selectivity than NaY synthesized from a metakaolin precursor. Ni/NaY-M and Ni/NaY-DM catalysts exhibited 100% selectivity toward CH₄

for the reactions up to 350°C. When the temperature was increased to 400°C, CO from the water-gas shift reaction was produced which consequently reduced the selectivity toward CH₄ to 94% on Ni/NaY-SM. The detrimental effect of a high reaction temperature was more significant for the Ni/NaY-M catalyst. Reaction at 550°C reduced the conversion of CO₂ to 30% and also the CH₄ selectivity to only 30%. Significant reduction in the productivity of CH₄ at temperatures of between 400 and 550°C for the Ni/NaY-M catalyst suggested that the catalysts have poor stability at high temperatures. For Ni/NaY-DM, the conversion of CO₂ to methane showed only slight

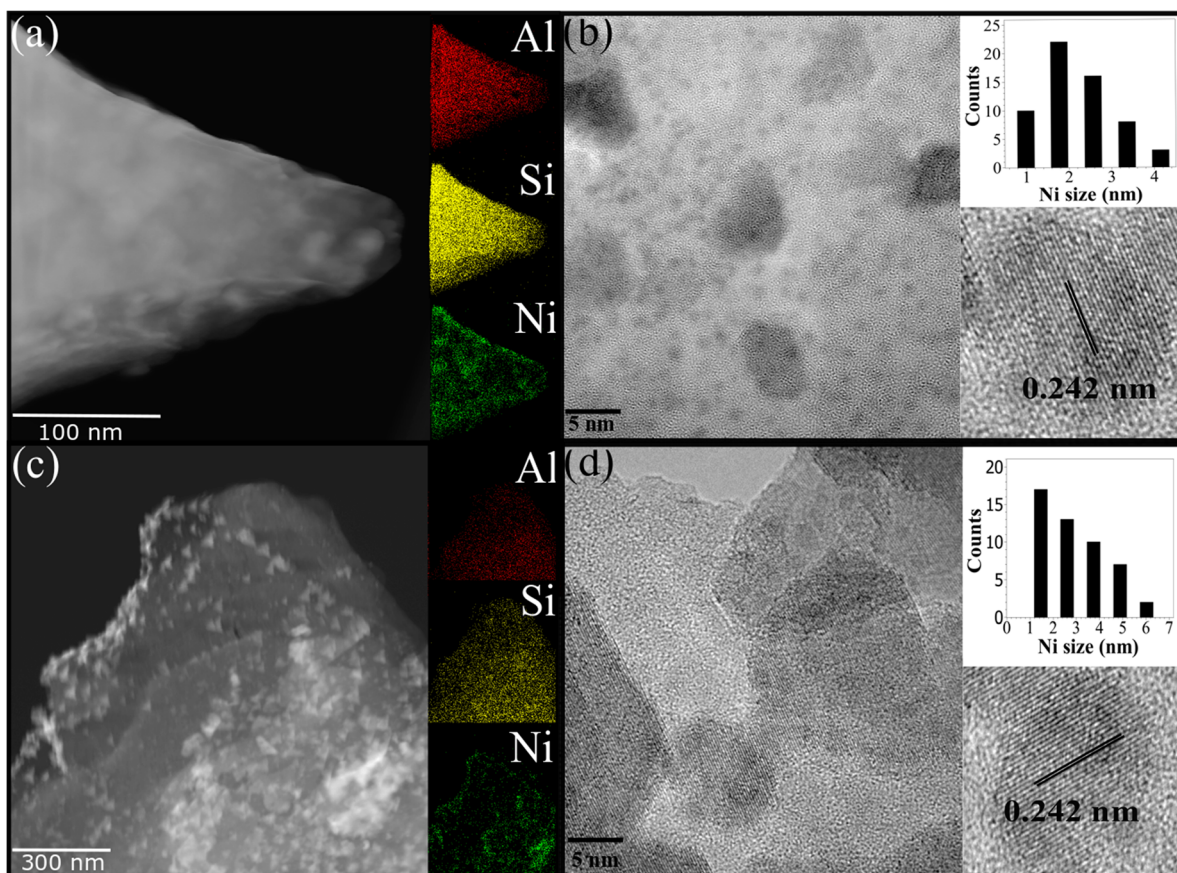


Fig. 5. **a** TEM analysis of Ni/NaY-DM, **b** HRTEM analysis of Ni/NaY-DM with its corresponding Ni particle-size distribution and Ni lattice spacing, **c** TEM analysis of Ni/NaY-M, and **d** HRTEM analysis of Ni/NaY-M with its corresponding Ni particle-size distribution and Ni lattice spacing

Table 4. Catalytic data from CO₂ methanation reaction at 400°C using Ni/NaY catalysts synthesized from dealuminated metakaolin (DM) and metakaolin (M)

Catalyst	Ni actual loading (%)	Ni diameter (nm)	χ CO ₂ (%)	S CH ₄ (%)	S CO (%)	Y CH ₄ (mmol/kg.h)	Y CO (mmol/kg.h)
5 wt.% Ni/NaY-DM	^a 6.3±0.2	^b 2.6±0.8	67	94	5.9	4412	276
5 wt.% Ni/ NaY-M	^a 4.6±0.2	^b 2.7±0.9	47	77	22.2	1784	525

^a Determined using AAS; ^b determined using HRTEM; S = selectivity; Y = yield

reduction at 500°C, which suggested that the NaY produced from dealuminated metakaolin provided a more stable support for Ni nanoparticles. The catalytic activity of Ni/NaY-DM was also compared with the activity of Ni nanoparticles supported on metal oxides SiO₂, Al₂O₃, MgO, on mesoporous silica SBA-15, on MCM-41, and on zeolites USY and ZSM-11 (Table 2). At a similar 5 wt.% loading of Ni, the CO₂ conversion of Ni/NaY-DM appeared lower than the conversion observed for Ni/ZSM-11, though Ni/NaY-DM showed 100% selectivity toward CH₄ at 350°C and only slightly reduced to 94% at 400°C.

Ni nanoparticles provided active sites for CO₂ dissociation during CO₂ hydrogenation reactions (Zhao et al. 2016; Fukuhara et al. 2017; Quindimil et al. 2018; Ewald et al. 2019). In the presence of H₂ as reducing agent, the dissociated CO₂ was further reduced to form methane (Bacariza et al. 2019). As no significant differences were observed between the sizes of Ni nanoparticles analyzed using HRTEM for Ni/NaY-DM and Ni/NaY-M, the enhanced catalytic performance of NaY-DM was suggested to be due to the increased surface area and pore volume of NaY, and the reduction of the Si/Al ratio of NaY. In general, the adsorption of CO₂ on NaY was

increased on any zeolite with large surface basicity (Walton et al. 2006). Reducing the concentration of Al increased the basicity of zeolite and enhanced the interaction of CO₂ with the basic oxygen framework (Bacariza et al. 2019). Synthesis of NaY from dealuminated metakaolin produced an aluminosilicate precursor containing little aluminum. Analysis by EDX (Table 2) revealed that the Si/Al ratios of NaY increased from 1.21 in NaY-M to 1.32 in NaY-DM, which implied a decrease in the Al content in the zeolite. Zeolite NaY produced from dealuminated metakaolin also exhibited a large surface area with well-defined octahedral structures. The rate-limiting step of the CO₂ methanation reaction involved the dissociation of the CO₂ bond followed by hydrogen insertion (Westermann et al. 2015). Adsorbed CO₂ reacted with the dissociated H₂ to form a monodentate formate intermediate on Ni⁰ which further hydrogenated to produce CH₄. The formate intermediate can also decompose on Ni⁰ via C–O bond dissociation, however, to form CO (Westermann et al. 2015). Catalytic activity of Ni/NaY-DM for CO₂ methanation showed high selectivity for CH₄ in comparison to Ni/NaY-M. The combination of a large surface area, well-defined structure, and low Si/Al ratios of

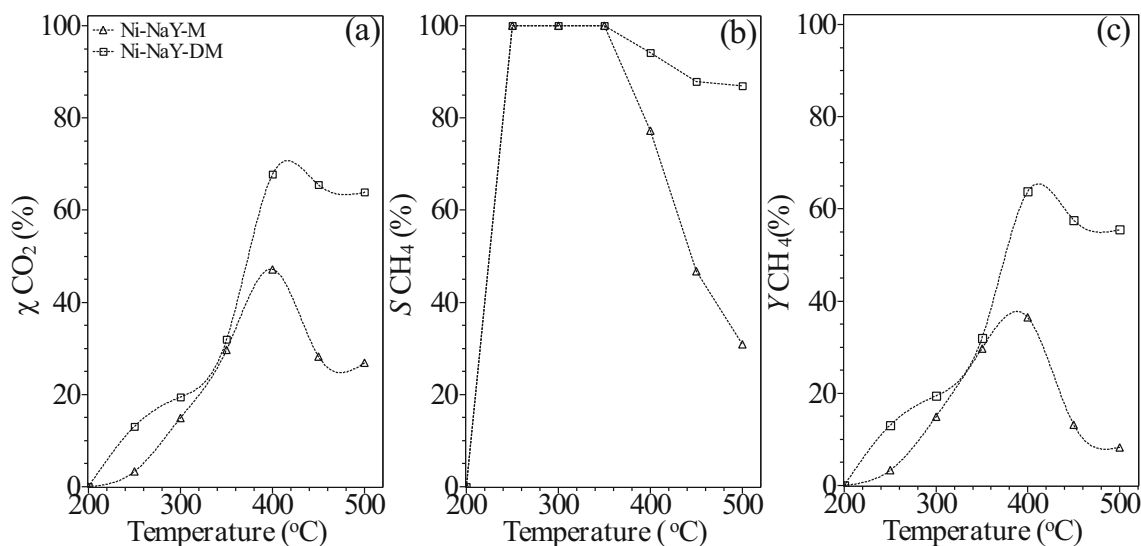


Fig. 6. Catalytic performance of 5 wt.% Ni-NaY-M synthesized from metakaolin and 5 wt.% Ni-NaY-DM from dealuminated metakaolin at various temperatures from 200 to 500°C. **a** Conversion of CO₂, **b** selectivity (S) of CH₄, and **c** yield (Y) of CH₄

NaY-DM is suggested to provide active support for stabilization of formate intermediates which allowed further hydrogenation to CH₄.

CONCLUSIONS

The structural properties and the catalytic activity of NaY synthesized from metakaolin (M) and dealuminated metakaolin (DM) were investigated as Ni supports for CO₂ methanation. Kaolin was transformed into metakaolin and subsequently treated with sulfuric acid to reduce the aluminum content of the metakaolin, yielding a sulfuric-acid soaked metakaolin (SM), then washed to remove excess sulfur to obtain the DM product. NaY synthesized from M produced non-uniform crystallite structures with 376 m²/g of surface area. Synthesis of NaY from DM significantly enhanced the surface area of NaY to ~500 m²/g with a well-defined octahedral structure. The presence of a large concentration of sulfur in the SM product produced NaY with a small surface area of ~260 m²/g. Ni/NaY catalysts produced from DM showed 67% of CO₂ conversion with 94% selectivity for methane as the product, both values of which were much greater than for the Ni/NaY catalysts synthesized from M. The enhanced catalytic activity was due to the large surface area, low sulfur content, well-defined crystallite structures, and low concentration of Al which facilitated CO₂ dissociation and stabilization of a formate intermediate for methane production, particularly for the reaction at high temperatures.

ACKNOWLEDGMENTS

The authors acknowledge the Ministries of Research, Technology, and Higher Education, Republic of Indonesia, for funding under PMDSU research fund number 5/EI/KP.PTNBH/2019 and PBK research fund number 841/PKS/ITS/2019 to D. Prasetyoko. The authors also acknowledge Universiti Brunei Darussalam Research Grant UBD/RSCH/URC/RG(b)/2019/012 for funding to H. Bahruji and UTM Transdisciplinary research grant (Grant no. 06G53) for funding to A. A. Jalil.

Funding

Funding sources are as stated in the acknowledgment.

Compliance with Ethical Statements

Conflict of Interest

The authors declare that they have no conflict of interest.

REFERENCES

- Alaba, P. A., Sani, Y. M., Mohammed, I. Y., Abakr, Y. A., & Wan Daud, W. M. A. (2017). Synthesis of hierarchical nanoporous HY zeolites from activated kaolin, a central composite design optimization study. *Advanced Powder Technology*, 28, 1399–1410. <https://doi.org/10.1016/j.apt.2017.03.008>
- Alkan, M., Hopa, Ç., Yilmaz, Z., & Güler, H. (2005). The effect of alkali concentration and solid/liquid ratio on the hydrothermal synthesis of zeolite NaA from natural kaolinite. *Microporous and Mesoporous Materials*, 86, 176–184. <https://doi.org/10.1016/j.micromeso.2005.07.008>
- Asghari, A., Khorrami, M. K., & Kazemi, S. H. (2019). Hierarchical H-ZSM5 zeolites based on natural kaolinite as a high-performance catalyst for methanol to aromatic hydrocarbons conversion. *Scientific Reports*, 9, 17526. <https://doi.org/10.1038/s41598-019-54089-y>
- Atzori, L., Cutrufello, M. G., Meloni, D., Monaci, R., Cannas, C., Gazzoli, D., Sini, M. F., Delana, P., & Rombi, E. (2017). CO₂ methanation on hard-templated NiO/CeO₂ mixed oxides. *International Journal of Hydrogen Energy*, 42, 20689–20702. <https://doi.org/10.1016/j.ijhydene.2017.06.198>
- Aziz, M. A. A., Jalil, A. A., Triwahyono, S., & Ahmad, A. (2015). CO₂ methanation over heterogeneous catalysts: recent progress and future prospects. *Green Chemistry*, 17, 2647–2663. <https://doi.org/10.1039/C5GC00119F>
- Azzolina-Jury, F., Bento, D., Henriques, C., & Thibault-Starzyk, F. (2017). Chemical engineering aspects of plasma-assisted CO₂ hydrogenation over nickel zeolites under partial vacuum. *Journal of CO₂ Utilization*, 22, 97–109. <https://doi.org/10.1016/j.jcou.2017.09.017>
- Bacariza, M. C., Graça, I., Bebiano, S. S., Lopes, J. M., & Henriques, C. (2018). Micro- and mesoporous supports for CO₂ methanation catalysis: A comparison between SBA-15, MCM-41 and USY zeolite. *Chemical Engineering Science*, 175, 72–83. <https://doi.org/10.1016/j.ces.2017.09.027>
- Bacariza, M. C., Graça, I., Lopes, J. M., & Henriques, C. (2019). Tuning zeolite properties towards CO₂ methanation: An overview. *ChemCatChem*, 11, 2388–2400. <https://doi.org/10.1002/cctc.201900229>
- Bahruji, H., Bowker, M., Hutchings, G., Dimitratos, N., Wells, P., Gibson, E., et al. (2016). Pd/ZnO catalysts for direct CO₂ hydrogenation to methanol. *Journal of Catalysis*, 343, 133–146. <https://doi.org/10.1016/j.jcat.2016.03.017>
- Bessa, R. D. A., Costa, L. D. S., Oliveira, C. P., Bohn, F., do Nascimento, R. F., Sasaki, J. M., & Loiola, A. R. (2017). Kaolin-based magnetic zeolites A and P as water softeners. *Microporous and Mesoporous Materials*, 245, 64–72. <https://doi.org/10.1016/j.micromeso.2017.03.004>
- Chen, L., Qian, J.-Y., Yang, C., Xu, P.-P., Zhu, D.-D., Zhong, J., He, M.-Y., Chen, Q., & Zhang, Z.-H. (2020). Direct synthesis of 5A zeolite from palygorskite: The influence of crystallization directing agent on the separation performance for hexane isomers. *Clays and Clay Minerals*, 68, 1–8. <https://doi.org/10.1007/s42860-019-00057-6>
- Colina, F. G., & Llorens, J. (2007). Study of the dissolution of dealuminated kaolin in sodium–potassium hydroxide during the gel formation step in zeolite X synthesis. *Microporous and Mesoporous Materials*, 100, 302–311. <https://doi.org/10.1016/j.micromeso.2006.11.013>
- Dong, J., Wang, X., Xu, H., Zhao, Q., & Li, J. (2007). Hydrogen storage in several microporous zeolites. *International Journal of Hydrogen Energy*, 32, 4998–5004. <https://doi.org/10.1016/j.ijhydene.2007.08.009>
- Doyle, A. M., Alismael, Z. T., Alabayati, T. M., & Abbas, A. S. (2017). High purity FAU-type zeolite catalysts from shale rock for biodiesel production. *Fuel*, 199, 394–402. <https://doi.org/10.1016/j.fuel.2017.02.098>
- Du, L., Ding, S., Li, Z., Lv, E., Lu, J., & Ding, J. (2018). Transesterification of castor oil to biodiesel using NaY zeolite-supported La₂O₃ catalysts. *Energy Conversion and Management*, 173, 728–734. <https://doi.org/10.1016/j.enconman.2018.07.053>
- Ewald, S., Kolbeck, M., Kratky, T., Wolf, M., & Hinrichsen, O. (2019). On the deactivation of Ni-Al catalysts in CO₂ methanation. *Applied Catalysis A: General*, 570, 376–386. <https://doi.org/10.1016/j.apcata.2018.10.033>
- Feng, A., Yu, Y., Mi, L., Cao, Y., Yu, Y., & Song, L. (2019). Synthesis and characterization of hierarchical Y zeolites using NH₄HF₂ as dealumination agent. *Microporous and Mesoporous Materials*, 280, 211–218. <https://doi.org/10.1016/j.micromeso.2019.01.039>

- Frusteri, F., Frusteri, L., Costa, F., Mezzapica, A., Cannilla, C., & Bonura, G. (2017). Methane production by sequential supercritical gasification of aqueous organic compounds and selective CO₂ methanation. *Applied Catalysis A: General*, *545*, 24–32. <https://doi.org/10.1016/j.apcata.2017.07.030>
- Fukuhara, C., Hayakawa, K., Suzuki, Y., Kawasaki, W., & Watanabe, R. (2017). A novel nickel-based structured catalyst for CO₂ methanation: A honeycomb-type Ni/CeO₂ catalyst to transform greenhouse gas into useful resources. *Applied Catalysis A: General*, *532*, 12–18. <https://doi.org/10.1016/j.apcata.2016.11.036>
- Gaidoumi, A. E., Benabdallah, A. C., Bali, B. E., & Kherbeche, A. (2018). Synthesis and characterization of zeolite HS using natural pyrophyllite as new clay source. *Arabian Journal for Science and Engineering*, *43*, 191–197. <https://doi.org/10.1007/s13369-017-2768-8>
- Ginter, D. M., Bell, A. T., & Radke, C. J. (1992). The effects of gel aging on the synthesis of NaY zeolite from colloidal silica. *Zeolites*, *12*, 742–749. [https://doi.org/10.1016/0144-2449\(92\)90126-A](https://doi.org/10.1016/0144-2449(92)90126-A)
- Graça, I., González, L. V., Bacariza, M. C., Fernandes, A., Henriques, C., Lopes, J. M., & Ribeiro, M. F. (2014). CO₂ hydrogenation into CH₄ on NiHNaUSY zeolites. *Applied Catalysis B: Environmental*, *147*, 101–110. <https://doi.org/10.1016/j.apcatb.2013.08.010>
- Graça, I., Bacariza, M. C., Fernandes, A., & Chadwick, D. (2018). Desilicated NaY zeolites impregnated with magnesium as catalysts for glucose isomerisation into fructose. *Applied Catalysis B: Environmental*, *224*, 660–670. <https://doi.org/10.1016/j.apcatb.2017.11.009>
- Holmberg, B. A., Wang, H., Norbeck, J. M., & Yan, Y. (2003). Controlling size and yield of zeolite Y nanocrystals using tetramethylammonium bromide. *Microporous and Mesoporous Materials*, *59*, 13–28. [https://doi.org/10.1016/S1387-1811\(03\)00271-3](https://doi.org/10.1016/S1387-1811(03)00271-3)
- Ifitahiyah, V. N., Prasetyoko, D., Hartati, Ni'Mah, Y. L., Bahruji, H., & Nur, H. (2019). Esterification of acetic acid and benzyl alcohol over Zeolite HX produced from Bangka Belitung kaolin. *Malaysian Journal of Analytical Sciences*, *23*, 524–533. <https://doi.org/10.17576/mjas-2019-2303-17>
- Kahraman, S., Önal, M., Sarıkaya, Y., & Bozdoğan, İ. (2005). Characterization of silica polymorphs in kaolins by X-ray diffraction before and after phosphoric acid digestion and thermal treatment. *Analytica Chimica Acta*, *552*, 201–206. <https://doi.org/10.1016/j.aca.2005.07.045>
- Klopprogge, J. T., Ruan, H., & Frost, R. L. (2001). Near-infrared spectroscopic study of basic aluminum sulfate and nitrate. *Journal of Materials Science*, *36*, 603–607. <https://doi.org/10.1023/A:1004860118470>
- Kovo, A. S., Hernandez, O., & Holmes, S. M. (2009). Synthesis and characterization of zeolite Y and ZSM-5 from Nigerian Ahoko Kaolin using a novel, lower temperature, metakaolinization technique. *Journal of Materials Chemistry*, *19*, 6207–6212. <https://doi.org/10.1039/B907554B>
- Li, Q., Zhang, Y., Cao, Z., Gao, W., & Cui, L. (2010). Influence of synthesis parameters on the crystallinity and Si/Al ratio of NaY zeolite synthesized from kaolin. *Petroleum Science*, *7*, 403–409. <https://doi.org/10.1007/s12182-010-0085-x>
- Li, N., Li, T., Liu, H., Yue, Y., & Bao, X. (2017). A novel approach to synthesize in-situ crystallized zeolite/kaolin composites with high zeolite content. *Applied Clay Science*, *144*, 150–156. <https://doi.org/10.1016/j.clay.2017.05.010>
- Luo, J., Zhang, H., & Yang, J. (2016). Hydrothermal synthesis of sodalite on alkali-activated coal fly ash for removal of lead ions. *Procedia Environmental Sciences*, *31*, 605–614. <https://doi.org/10.1016/j.proenv.2016.02.105>
- Mu, L., Feng, W., Zhang, H., Hu, X., & Cui, Q. (2019). Synthesis and catalytic performance of a small crystal NaY zeolite with high SiO₂/Al₂O₃ ratio. *RSC Advances*, *9*, 20528–20535. <https://doi.org/10.1039/C9RA03324F>
- Ptáček, P., Šoukal, F., Opravil, T., Nosková, M., Havlica, J., & Brandšter, J. (2011). Mid-infrared spectroscopic study of crystallization of cubic spinel phase from metakaolin. *Journal of Solid State Chemistry*, *184*, 2661–2667. <https://doi.org/10.1016/j.jssc.2011.07.038>
- Qoniah, I., Prasetyoko, D., Bahruji, H., Triwahyono, S., Jalil, A. A., Suprpto, H., & Purbaningtias, T. E. (2015). Direct synthesis of mesoporous aluminosilicates from Indonesian kaolin clay without calcination. *Applied Clay Science*, *118*, 290–294. <https://doi.org/10.1016/j.clay.2015.10.007>
- Quindimil, A., De-La-Torre, U., Pereda-Ayo, B., González-Marcos, J. A., & González-Velasco, J. R. (2018). Ni catalysts with La as promoter supported over Y- and BETA- zeolites for CO₂ methanation. *Applied Catalysis B: Environmental*, *238*, 393–403. <https://doi.org/10.1016/j.apcatb.2018.07.034>
- Rakshit, S., Ghosh, S., Chall, S., Mati, S. S., Moulik, S. P., & Bhattacharya, S. C. (2013). Controlled synthesis of spin glass nickel oxide nanoparticles and evaluation of their potential antimicrobial activity: A cost effective and eco friendly approach. *RSC Advances*, *3*, 19348–19356. <https://doi.org/10.1039/C3RA42628A>
- Rasouli, H. R., Golestani-fard, F., Mirhabibi, A. R., Nasab, G. M., Mackenzie, K. J. D., & Shahraki, M. H. (2015). Fabrication and properties of microporous metakaolin-based geopolymer bodies with polylactic acid (PLA) fibers as pore generators. *Ceramics International*, *41*, 7872–7880. <https://doi.org/10.1016/j.ceramint.2015.02.125>
- Sperinck, S., Raiteri, P., Marks, N., & Wright, K. (2011). Dehydroxylation of kaolinite to metakaolin—a molecular dynamics study. *Journal of Materials Chemistry*, *21*, 2118–2125. <https://doi.org/10.1039/C0JM01748E>
- Sri Rahayu, E., Subiyanto, G., Imanuddin, A., Wiranto, Nadina, S., Ristiani, R., Suhermina, & Yuniarti, E. (2018). Kaolin as a source of silica and alumina for synthesis of zeolite Y and amorphous silica alumina. *MATEC Web Conference*, *156*.
- Wahyuni, T., Prasetyoko, D., Suprpto, S., Qoniah, I., Bahruji, H., Dawam, A., Triwahyono, S., & Jalil, A. A. (2019). Direct synthesis of sodalite from Indonesian kaolin for adsorption of Pb²⁺ solution, kinetics, and isotherm approach. *Bulletin of Chemical Reaction Engineering and Catalysis*, *14*, 502–512. <https://doi.org/10.9767/bcrec.14.3.2939.502-512>
- Walton, K. S., Abney, M. B., & Douglas LeVan, M. (2006). CO₂ adsorption in Y and X zeolites modified by alkali metal cation exchange. *Microporous and Mesoporous Materials*, *91*, 78–84. <https://doi.org/10.1016/j.micromeso.2005.11.023>
- Wang, P., Zha, F., Yao, L., & Chang, Y. (2018). Synthesis of light olefins from CO₂ hydrogenation over (CuO-ZnO)-kaolin/SAPO-34 molecular sieves. *Applied Clay Science*, *163*, 249–256. <https://doi.org/10.1016/j.clay.2018.06.038>
- Weitkamp, J. & Hunger, M. (2005). Preparation of zeolites via the dry-gel synthesis method. In: *Oxide Based Materials: New Sources, Novel Phases, New Applications* (A. Gamba, C. Colella, and S. Coluccia, Editors). Studies in Surface Science and Catalysis (Vol. 155). Amsterdam, Elsevier, pp. 1–12.
- Westermann, A., Azambre, B., Bacariza, M. C., Graça, I., Ribeiro, M. F., Lopes, J. M., & Henriques, C. (2015). Insight into CO₂ methanation mechanism over NiUSY zeolites: An operando IR study. *Applied Catalysis B: Environmental*, *174–175*, 120–125. <https://doi.org/10.1016/j.apcatb.2015.02.026>
- Zhang, Z., Tian, Y., Zhang, L., Hu, S., Xiang, J., Wang, Y. et al. (2019). Impacts of nickel loading on properties, catalytic behaviors of Ni/γ-Al₂O₃ catalysts and the reaction intermediates formed in

- methanation of CO₂. *International Journal of Hydrogen Energy*, *44*, 9291–9306. <https://doi.org/10.1016/j.ijhydene.2019.02.129>
- Zhao, K., Li, Z., & Bian, L. (2016). CO₂ methanation and co-methanation of CO and CO₂ over Mn-promoted Ni/Al₂O₃ catalysts. *Frontiers of Chemical Science and Engineering*, *10*, 273–280. <https://doi.org/10.1007/s11705-016-1563-5>
- Zhou, G., Wu, T., Zhang, H., Xie, H., & Feng, Y. (2014). Carbon dioxide methanation on ordered mesoporous CO/KIT-6 CATALYST. *Chemical Engineering Communications*, *201*, 233–240. <https://doi.org/10.1080/00986445.2013.766881>

(Received 7 November 2019; revised 24 June 2020; AE: Binoy Sarkar)